Expanded Methods

Imaging

Quartz crystals bearing melt inclusions were selected randomly for tomographic imaging from crystal separates. All imaging was conducted on the GSECARS-13 bending magnet beamline of the Advanced Photon Source (APS) at Argonne National Laboratory (Chicago, IL), following the procedures of Pamukcu et al. (2013). The data provided here were obtained from five Ohakuri-Mamaku (OHK, MAM) ignimbrite crystals (Bégué et al., 2014), fifteen phase 10 (ORN-067) and five phase 1 (P1577) airfall Oruanui crystals (Wilson, 2001), and thirteen Bishop crystals (BB08: airfall F6/F7, BC17: ignimbrite Ig2E, F815: airfall F8; Wilson and Hildreth, 1997).

To compare melt inclusion faceting times and growth rates with those from Ti diffusion chronometry, we made measurements using both methods on a subset of Ohakuri-Mamaku crystals. Initially, ~80 quartz crystals were selected randomly from Ohakuri-Mamaku pumice clasts and imaged with tomography. After inspecting these tomograms, we selected ~35 of the crystals to image for Ti zoning. Crystals were selected based on: (a) if they contained fully-enclosed inclusions of resolvable size (the image processing procedures can only be used on fully-enclosed inclusions >10 pixels in diameter), and (b) how many inclusions they contained (we aimed to expose as many inclusions as possible in 2-D sectioning). Each crystal was mounted individually in epoxy (c-axis vertical), sectioned to expose melt inclusions, and imaged with cathodolminescence (CL) on a scanning electron microscope (SEM). We aimed to assess times from boundaries as close to or containing melt inclusions of interest. However, at times imaging revealed complex zoning and artifacts due to unexposed melt inclusions (see below, Fig.

DR4), and we avoided these areas for the sake of obtaining the best possible comparison between faceting and diffusion chronometry. In some cases, melt inclusions of interest were unfortunately polished through, making it difficult or impossible to know which zones contained them. Ultimately, five of the imaged crystals provided useful results for comparison.

Previous work has shown that CL intensity can be a good proxy for Ti contents in quartz (Cherniak et al., 2007; Spear and Wark, 2009; Gualda et al., 2012a; Leeman et al., 2012), and we verified this in a subset of our crystals by comparing CL images with Ti maps obtained by x-ray microprobe on the GSECARS-13 insertion device beamline at APS. We find that the large variations in CL zoning that are most relevant to our time calculations correlate well with Ti; however, subtle variations (i.e. fine oscillatory zoning) do not (Fig. DR1). Given the correlation between Ti and CL in our samples, and the fact that CL imaging on an SEM provides considerably better spatial resolution than the x-ray microprobe used for Ti mapping, we use CL intensity variations to derive crystallization times.

In CL imaging, the incident electron beam energy constrains both the signal-to-noise ratio (better at higher energy) and smoothing due to electron scattering within the sample (better at lower energy). We find that a 15 kV beam provides sufficient contrast and adequate spatial resolution for the timescales of interest in these crystals (Fig. DR1). We note that unexposed portions of melt inclusions can affect CL intensity, creating noticeably darker or lighter areas inconsistent with other zoning, and we avoided these areas in our analysis (Fig. DR4).

Melt Inclusion Faceting & Diffusion Chronometry

To obtain timescale estimates from these two approaches, we use the equations developed and explained in detail by Gualda et al. (2012a; see also Fig. DR1). We use temperatures of 780 °C (Ohakuri-Mamaku; Bégué et al., 2014), 770 °C (Oruanui; Allan et al.,

2013) and 750 °C (Bishop Tuff; Cherniak et al., 2007) for T and to calculate D_{Si} and D_{Ti} (Baker, 1991; Gualda et al. 2012a). The ΔV parameter used for faceting calculations is the total volume of material moved during the faceting process and is calculated from the number of pixels that protrude from an ellipsoid of the same volume, which is determined during image processing. All inclusions used for faceting calculations are fully-enclosed and of resolvable size in tomographic images. For a given Oruanui or Bishop crystal, all inclusions that fulfilled these requirements were assessed. For Ohakuri-Mamaku, the inclusions selected for analysis fulfilled these requirements but were also those exposed when crystals were sectioned after tomographic imaging. This totals to: 15 inclusions from Ohakuri-Mamaku crystals, 44 inclusions from Oruanui crystals, and 107 inclusions from Bishop Tuff crystals.

For time estimates from diffusion chronometry, we collect 11 parallel diffusion profiles (5 on each side of the originally drawn profile) spaced in one pixel increments. We then calculate timescales from each individual profile and an average profile. We remove any individual profiles that appear to be severely affected by aberrations in the image (e.g. extraneous bright or dark pixels – noise) or interact with other features in the crystal that affect intensities (e.g. melt inclusions). We report estimates from the average profile. Boundaries in Ohakuri-Mamaku crystals used for diffusion chronometry were: (a) those that showed distinct CL contrast on either side, as these are correlated with Ti, (b) traceable through much of the image, and (c) not irregular (i.e. not wavy). Ideally, boundaries of zones that contained melt inclusions used for faceting calculations were also assessed.

As noted in the main text, the error calculations for our timescale estimates take a 60 °C temperature range into account. If the system cools enough that diffusion is unable to proceed (e.g. the system enters the subsolidus realm), the processes being measured will essentially stop.

Our calculations do not take such extreme variations into account; however, in this scenario, the resultant timescales are still maxima for the accumulation of the final eruptible melt-rich magma body, which is what we focus on here. In other words, melt inclusion faceting and diffusional relaxation of compositional profiles will proceed immediately after entrapment and for any time spent at magmatic temperatures. Consequently, the time estimates retrieved from these features would be equal to (no time spent subsolidus) or overestimate (time spent subsolidus) the final accumulation time. If the temperature of the system increased but did not result in resorption of melt inclusions or boundaries, the times we would retrieve would be shorter than the real times; however, we do not see strong indications of such large temperature variations in our crystals (e.g. extremely bright CL areas) that are not accounted for by the 60 °C temperature range included in the error calculations.

Growth rates were calculated using the calculated time and nearest distance to the crystal edge for a given melt inclusion (determined in 3-D from tomographic images) or zone boundary (determined in 2-D from CL images). In some cases, crystals imaged with tomography were not euhedral, such that the nearest edge to a given melt inclusion calculated by the image processing software was a broken edge of the crystal. We do not include these values in our dataset. In the case of CL images, the nearest edge to a given inclusion or boundary may be one in the third dimension not visible in the 2-D image.

Rhyolite-MELTS modeling

Rhyolite-MELTS calculations were performed at constant pressure, in equilibrium mode, with oxygen fugacity fixed at the Ni-NiO buffer, under water-saturated conditions. Crystallization pressures used for the simulations were based on previous work on these systems, which is summarized by Gualda and Ghiorso (2013).

REFERENCES CITED

Gualda, G. A. R., and Ghiorso, M. S., 2013, Low pressure origin of high-silica rhyolites: Journal of Geology, v. 121, p. 537-545, doi: 10.1086/671395.

Example schematic of melt inclusion time plot

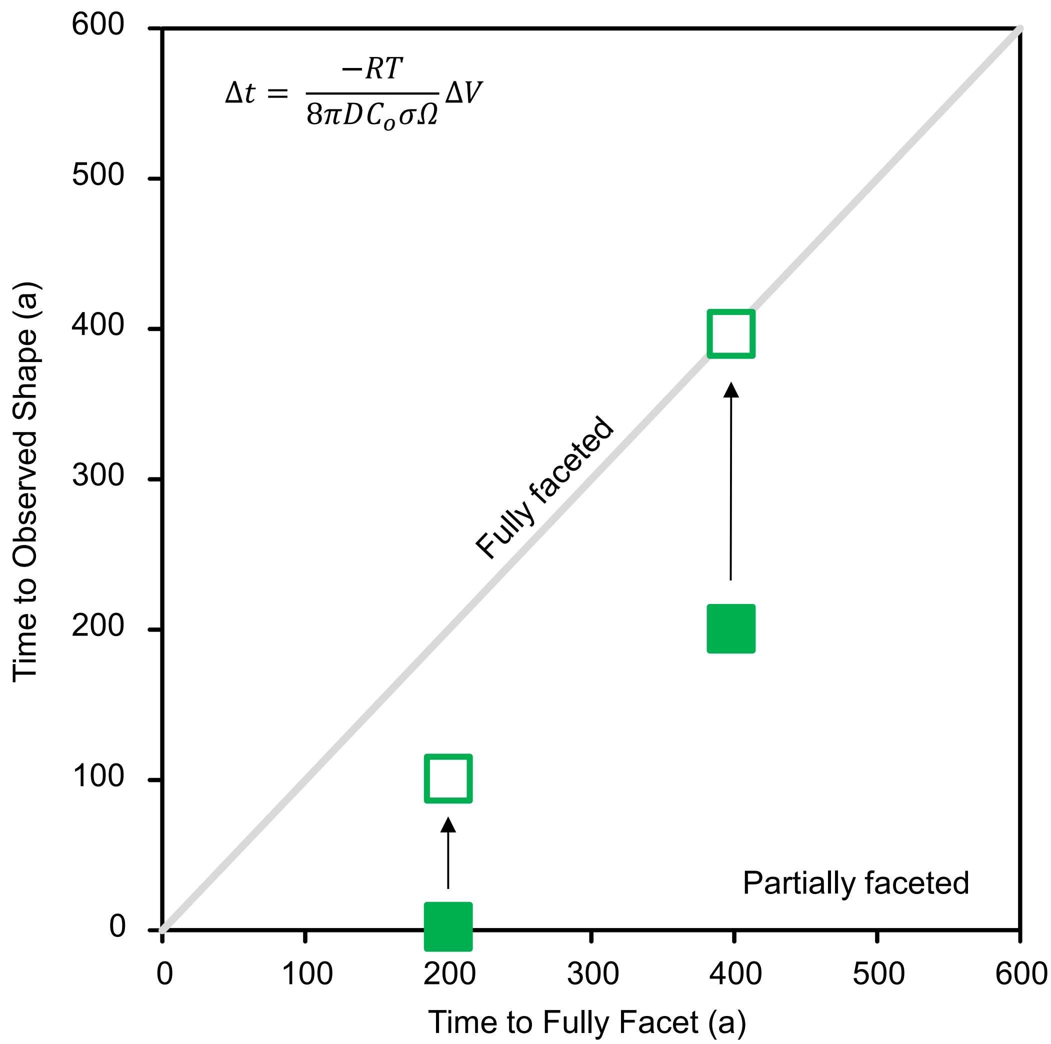

Figure DR1. Schematic showing evolution of melt inclusion shape through time. Fully faceted inclusions will lie on the 1:1 line, at which the time to achieve full faceting is equal to the time calculated from image processing (i.e., current degree of faceting). At time = 0, an inclusion will lie on the x-axis (no faceting has occurred), and as time passes, the inclusion will move vertically from the initial position on the x-axis. The initial position on the x-axis is a function of the inclusion size – smaller inclusions will facet more rapidly than large inclusions (less material to diffuse to achieve full faceting), so they will become fully faceted in less time. Equation used to calculate faceting time is from Gualda et al. 2012a.

<u>Variables in faceting time calculation</u>

R: Ideal gas constant
T: temperature
D: diffusion coefficient for Si in melt
C_0: solubility of a particle of infinite radius
σ: surface free energy
Ω: molar volume of phase of interest
ΔV: volume of melt inclusion that is moved in faceting processes (determined from tomography; see text for details)

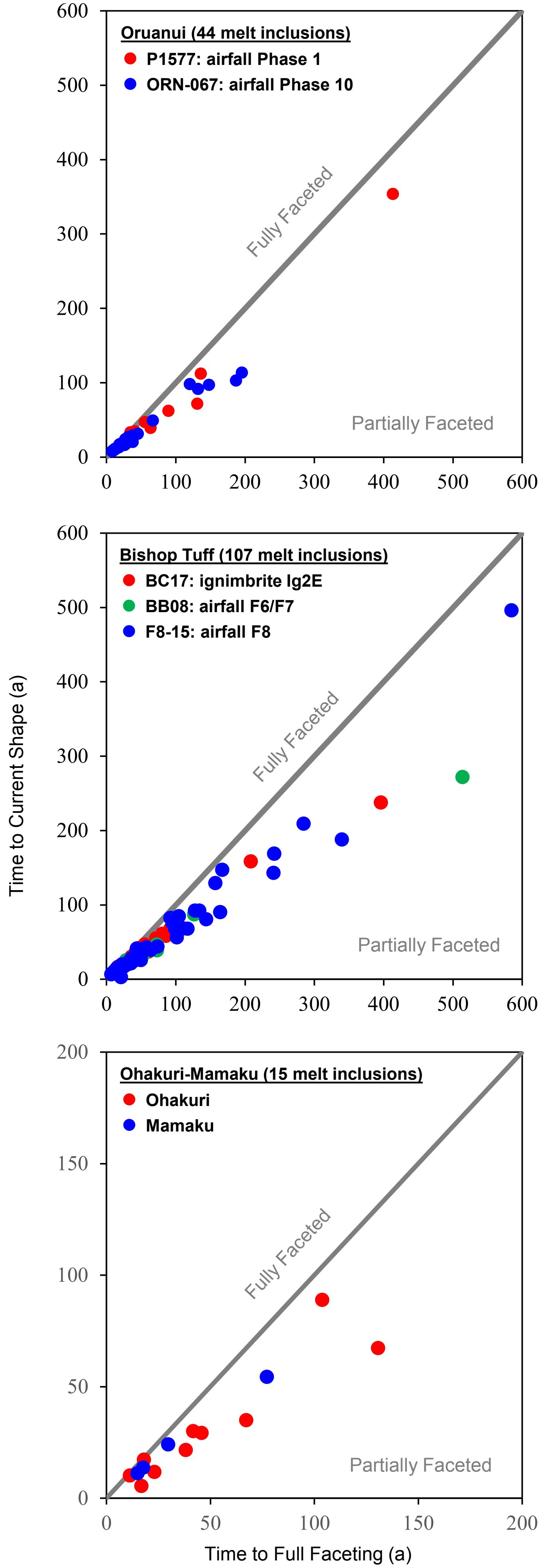

Figure DR1, continued. Faceting times for individual eruptive units studied

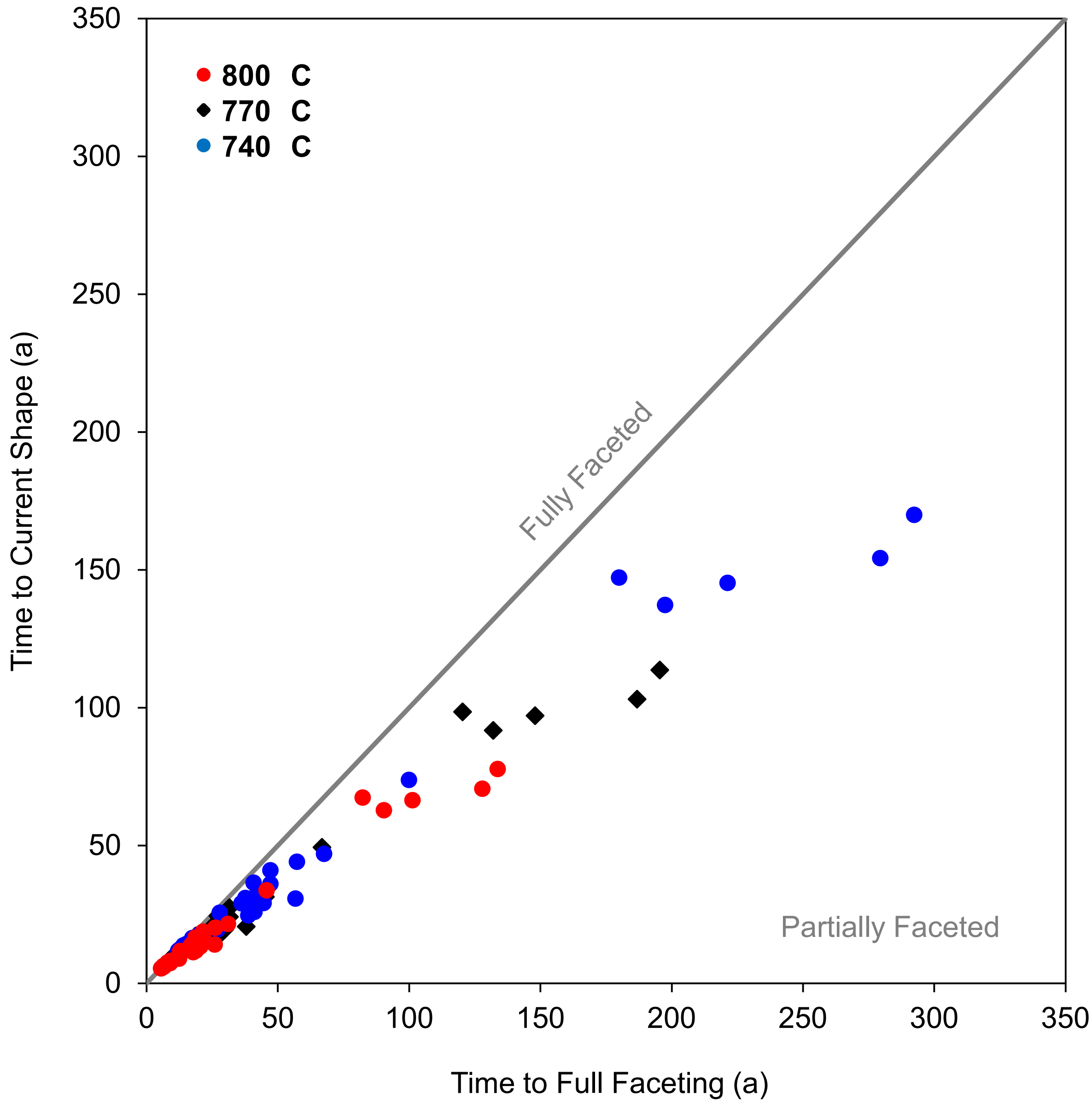

Figure DR1, continued. Time estimates for ORN-067 over a range of temperatures (±30 °C).

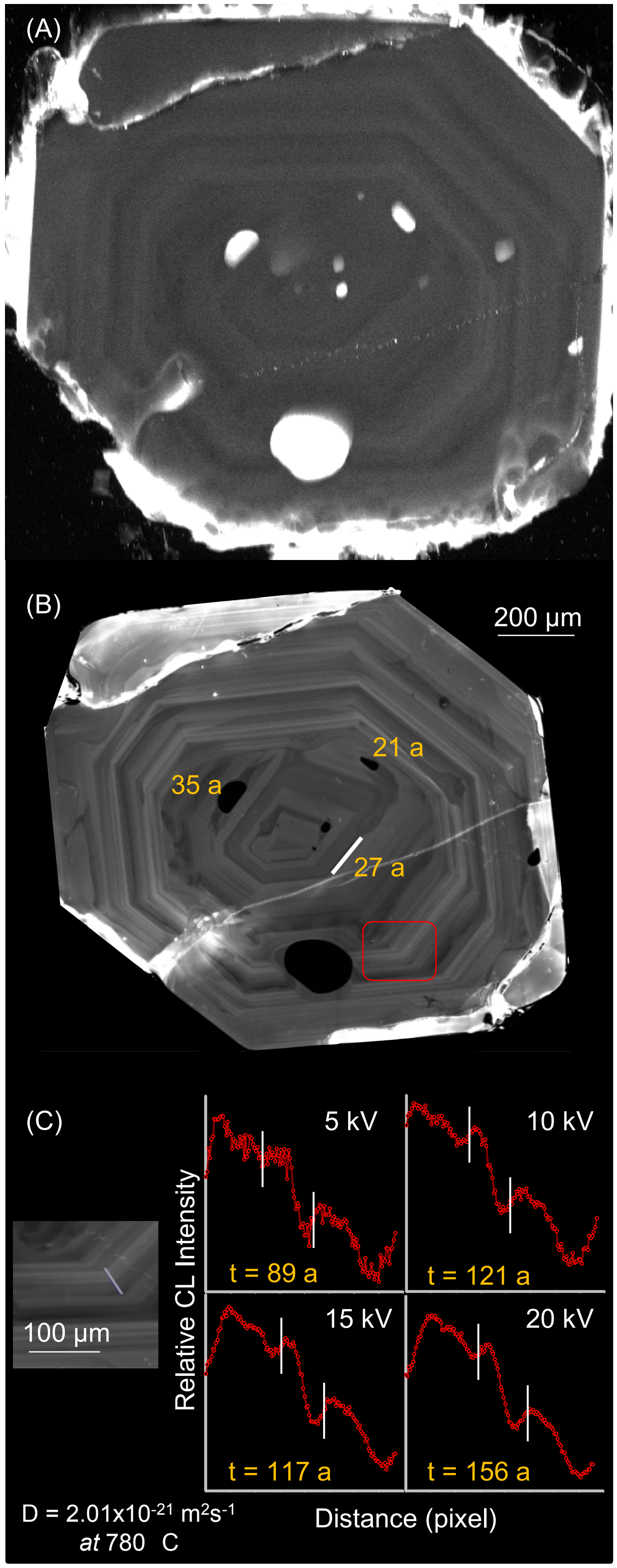

Figure DR2. Quartz zoning, melt inclusion faceting and diffusional relaxation times from an Ohakuri-Mamaku crystal. (A) Titanium map of quartz crystal in (B). (B) CL image of crystal with times from faceting (black melt inclusions) and diffusional relaxation (boundary highlighted by white line). Red box indicates area characterized in (C). (C) Comparison of diffusion profiles obtained from CL images collected with varying beam energies. Dashed lines represent profile portion fit for timescales estimates (noted in yellow).

Figure DR3. Cathodoluminescence images of Ohakuri-Mamaku quartz crystals, with timescale and growth rate estimates from melt inclusion faceting and diffusion chronometry. Scale bars are 200 μm.

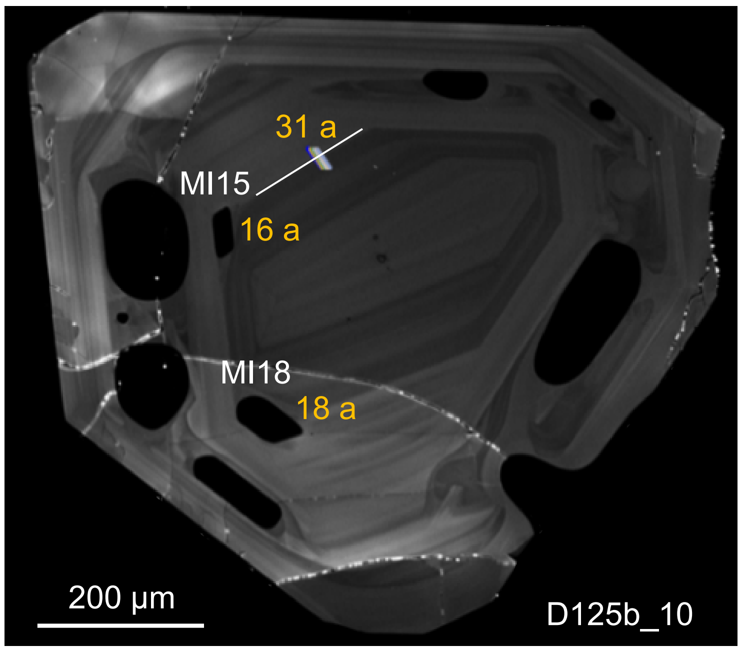

D125b_10	Time (a)	Time (s)	Distance to Nearest Edge (pixel)	Image Resolution (μm/pixel)	Distance to Nearest Edge (m)	Growth Rate (m/s)
MI 15 (tomography)	16	5.05×10^{8}	101.4	2.76	2.80×10^{-4}	5.55×10^{-13}
MI 18 (tomography)	18	5.68×10^{8}	113.5	2.76	3.13×10^{-4}	5.52×10^{-13}
Diffusion Profile (CL image)	31	9.78×10^{8}	32.3	2.06	6.66×10^{-5}	6.81×10^{-14}

Figure DR3, continued. Cathodoluminescence images of Ohakuri-Mamaku quartz crystals, with timescale and growth rate estimates from melt inclusion faceting and diffusion chronometry. Scale bars are 200 μm.

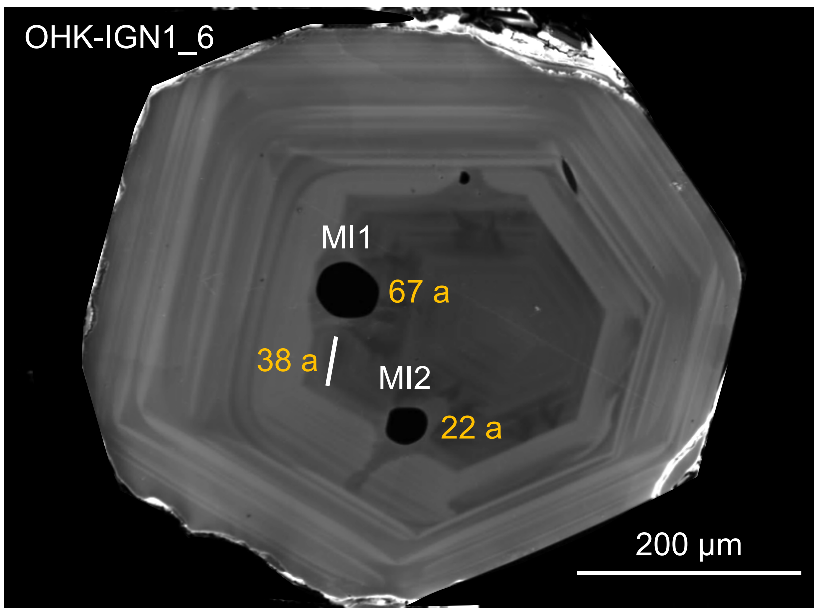

OHK-IGN1_6	Time (a)	Time (s)	Distance to Nearest Edge (pixel)	Image Resolution (μm/pixel)	Distance to Nearest Edge (m)	Growth Rate (m/s)
MI 1 (tomography)	67	2.11×10^{9}	51.2	2.76	1.41×10^{-4}	6.68×10^{-14}
MI 2 (tomography)	22	6.94×10^{8}	38.4	2.76	1.06×10^{-4}	1.53×10^{-13}
Diffusion Profile (CL image)	38	1.20×10^{9}	168.9	1.65	2.79×10^{-4}	2.33×10^{-13}

Figure DR3, continued. Cathodoluminescence images of Ohakuri-Mamaku quartz crystals, with timescale and growth rate estimates from melt inclusion faceting and diffusion chronometry. Scale bars are 200 μm.

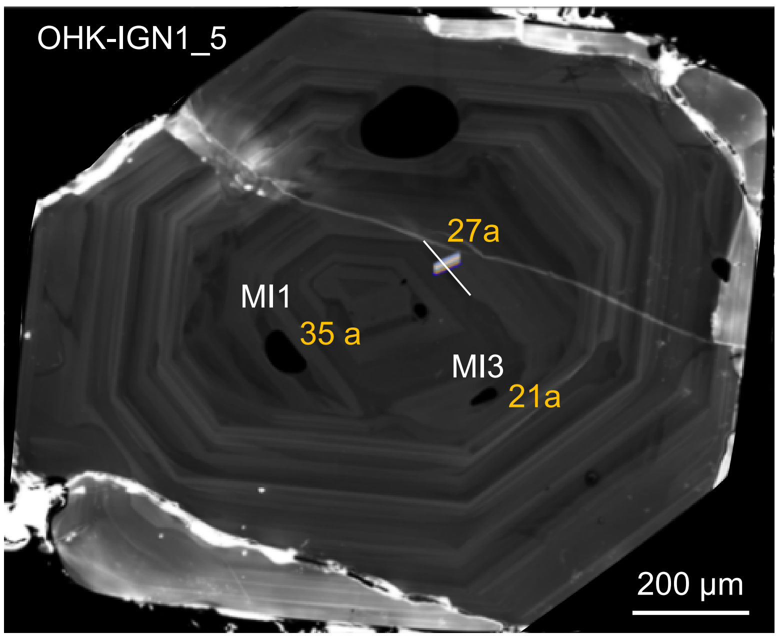

OHK-IGN1_5	Time (a)	Time (s)	Distance to Nearest Edge (pixel)	Image Resolution (μm/pixel)	Distance to Nearest Edge (m)	Growth Rate (m/s)
MI 1 (tomography)	35	1.10×10^{9}	139.6	2.76	3.85×10^{-4}	3.49×10^{-13}
MI 3 (tomography)	21	6.62×10^{8}	116.1	2.76	3.20×10^{-4}	4.84×10^{-13}
Diffusion Profile (CL image)	27	8.51×10^{8}	203.9	3.03	6.18×10^{-4}	7.25×10^{-13}

Figure DR3, continued. Cathodoluminescence images of Ohakuri-Mamaku quartz crystals, with timescale and growth rate estimates from melt inclusion faceting and diffusion chronometry. Scale bars are 200 μm.

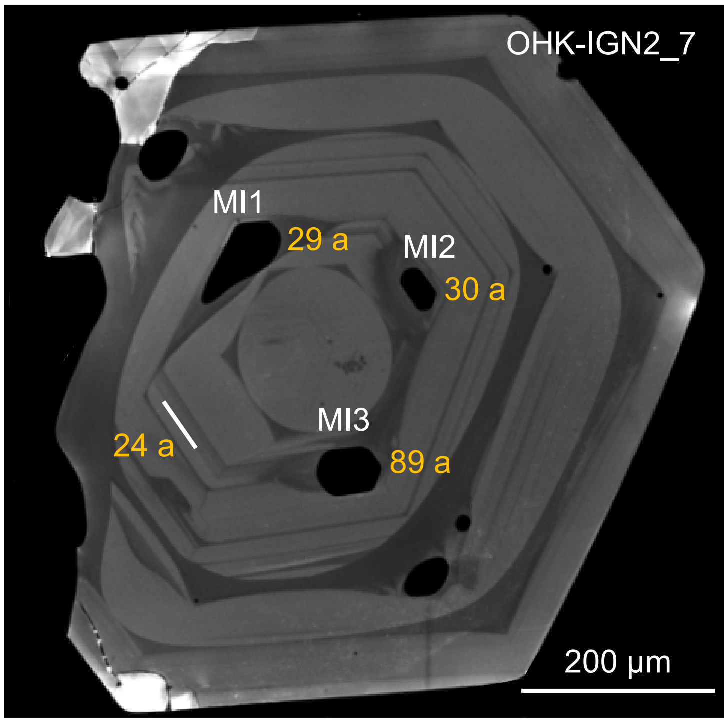

OHK-IGN2_7	Time (a)	Time (s)	Distance to Nearest Edge (pixel)	Image Resolution (μm/pixel)	Distance to Nearest Edge (m)	Growth Rate (m/s)
MI 1 (tomography)	29	9.15×10^{8}	67.8	2.76	1.87×10^{-4}	2.05×10^{-13}
MI 2 (tomography)	30	9.46×10^{8}	91.5	2.76	2.53×10^{-4}	2.67×10^{-13}
MI 3 (tomography)	89	2.81×10^{9}	89.7	2.76	2.47×10^{-4}	8.82×10^{-14}
Diffusion Profile (CL image)	24	7.57×10^{8}	115.4	1.89	2.18×10^{-4}	2.88×10^{-13}

Figure DR3, continued. Cathodoluminescence images of Ohakuri-Mamaku quartz crystals, with timescale and growth rate estimates from melt inclusion faceting and diffusion chronometry. Scale bars are 200 μm.

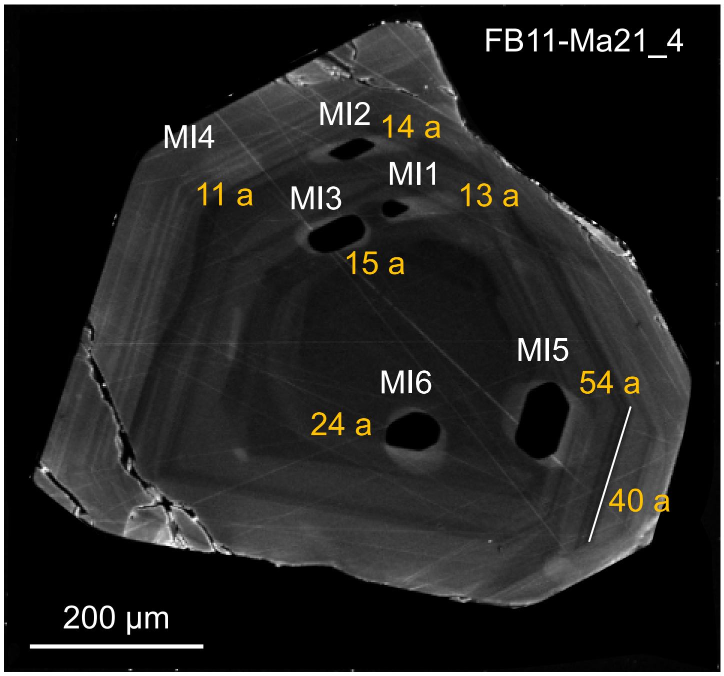

FB11-Ma21_4	Time (a)	Time (s)	Distance to Nearest Edge (pixel)	Image Resolution (μm/pixel)	Distance to Nearest Edge (m)	Growth Rate (m/s)
MI 1 (tomography)	13	4.10×10^{8}	57.3	2.76	1.58×10^{-4}	3.86×10^{-13}
MI 2 (tomography)	14	4.42×10^{8}	45.0	2.76	1.24×10^{-4}	2.18×10^{-13}
MI 3 (tomography)	15	4.73×10^{8}	69.2	2.76	1.91×10^{-4}	4.04×10^{-13}
MI 4 (tomography)	11	3.47×10^{8}	39.7	2.76	1.10×10^{-4}	3.16×10^{-13}
MI 5 (tomography)	54	1.70×10^{9}	65.5	2.76	1.81×10^{-4}	1.06×10^{-13}
MI 6 (tomography)	24	7.57×10^{8}	66.2	2.76	1.83×10^{-4}	2.42×10^{-13}
Diffusion Profile (CL image)	40	1.26×10^{9}	32.3	2.06	6.66×10^{-5}	5.28×10^{-14}

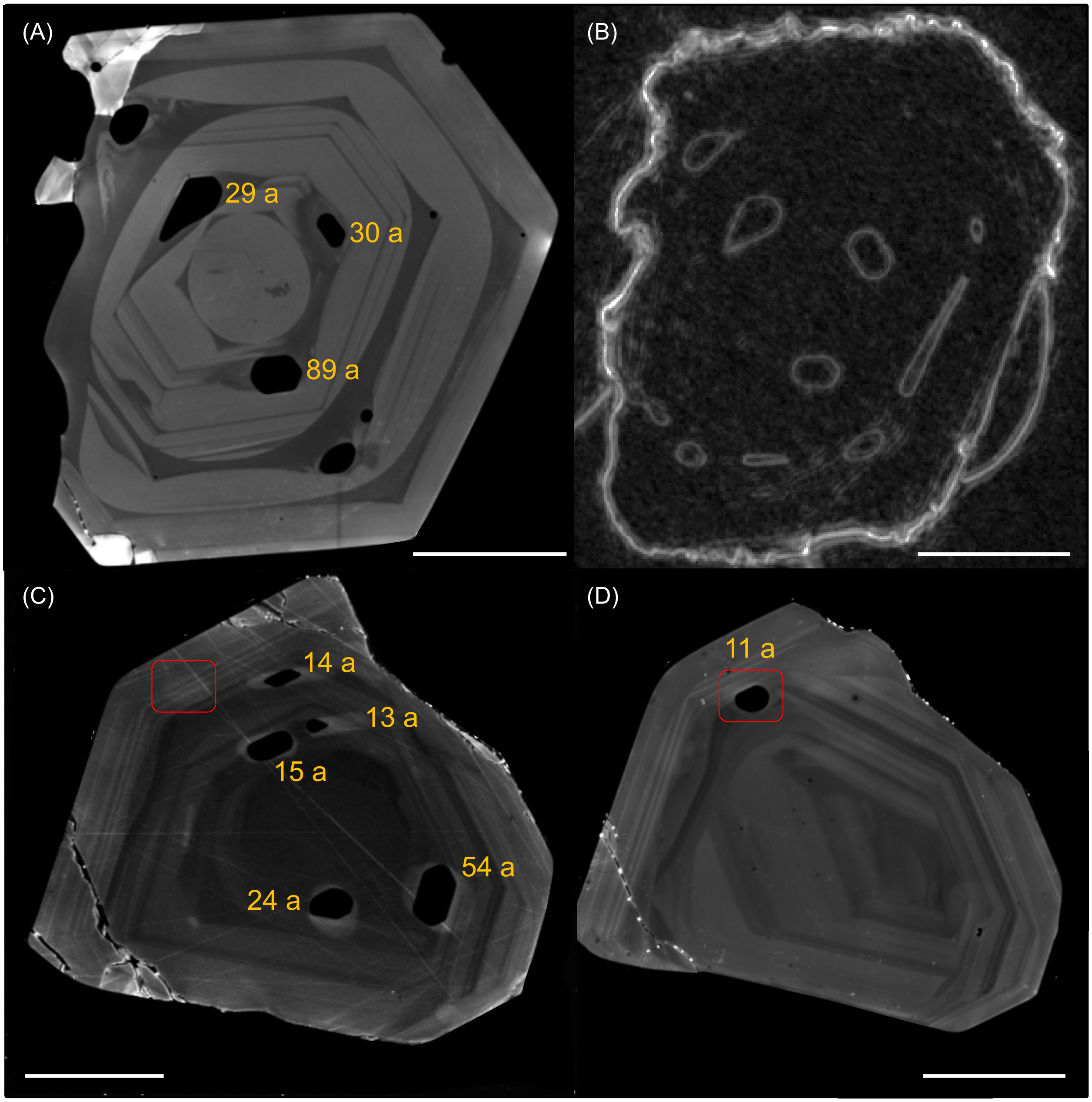

Figure DR4. CL images and tomogram slices of quartz crystal. (A, B) CL image and tomogram slice, respectively, of the same quartz crystal at approximately the same position in the grain. (C, D) CL images of a quartz crystal successively polished to expose occluded melt inclusion (see region marked by red triangle). Unexposed melt inclusions appear to affect CL intensity in some cases (dark inconsistent swaths, bright halos around melt inclusions). Times from faceting and diffusional relaxation are given in yellow. Scale bars = 200 μm.

Table DR1

P1577_4

	ΔV	um^3	m^3	T (K)	Δt (s)	Δt (yr)	Distance to Nearest Edge (m)	Growth Rate (m/s)
MI1	1226.51	2.61E+04	2.61E-14	1043.15	2.27E+09	**72**	2.13E-04	9.41E-14
MI4	190.00	4.04E+03	4.04E-15	1043.15	3.54E+09	**112**		
MI11	26.00	5.53E+02	5.53E-16	1043.15	1.96E+09	**62**	1.12E-04	5.71E-14

P1577_6

	ΔV	um^3	m^3	T (K)	Δt (s)	Δt (yr)		
MI3	315.666	6.71E+03	6.71E-15	1043.15	5.84E+08	**19**	1.04E-04	4.48E-13
MI8	6041.18	1.28E+05	1.28E-13	1043.15	1.12E+10	**354**	1.90E-04	4.25E-14
MI9	568.501	1.21E+04	1.21E-14	1043.15	1.05E+09	**33**	1.80E-04	4.28E-13
MI10	298.5	6.34E+03	6.34E-15	1043.15	5.52E+08	**17**	1.77E-04	8.00E-13

P1577_8

	ΔV	um^3	m^3	T (K)	Δt (s)	Δt (yr)		
MI2	516.83	1.10E+04	1.10E-14	1043.15	9.56E+08	**30**		
MI5	305.50	6.49E+03	6.49E-15	1043.15	5.65E+08	**18**		
MI8	802.67	1.71E+04	1.71E-14	1043.15	1.48E+09	**47**		
MI9	593.00	1.26E+04	1.26E-14	1043.15	1.10E+09	**35**	2.20E-04	2.01E-13

P1577_12

	ΔV	um^3	m^3	T (K)	Δt (s)	Δt (yr)		
MI1	669.16	1.42E+04	1.42E-14	1043.15	1.24E+09	**39**	8.79E-05	7.10E-14

ORN-067_1

	ΔV	um^3	m^3	T (K)	Δt (s)	Δt (yr)		
MI1	332.67	7.07E+03	7.07E-15	1043.15	6.15E+08	**19**	1.98E-04	3.22E-13
MI5	352.67	7.50E+03	7.50E-15	1043.15	6.52E+08	**21**	1.57E-04	2.42E-13
MI6	536.00	1.14E+04	1.14E-14	1043.15	9.91E+08	**31**	2.00E-04	2.02E-13
MI10	334.17	7.10E+03	7.10E-15	1043.15	6.18E+08	**20**	1.98E-04	3.21E-13
MI11	503.34	1.07E+04	1.07E-14	1043.15	9.31E+08	**30**	1.44E-04	1.55E-13
MI12	296.17	6.29E+03	6.29E-15	1043.15	5.48E+08	**17**	1.15E-04	2.10E-13
MI13	162.67	3.46E+03	3.46E-15	1043.15	3.01E+08	**10**	2.82E-04	9.39E-13
MI14	1679.33	3.57E+04	3.57E-14	1043.15	3.11E+09	**98**	1.25E-04	4.04E-14
MI17	292.50	6.22E+03	6.22E-15	1043.15	5.41E+08	**17**	1.20E-04	2.21E-13
MI19	290.50	6.17E+03	6.17E-15	1043.15	5.37E+08	**17**	1.20E-04	2.23E-13
MI20	416.00	8.84E+03	8.84E-15	1043.15	7.69E+08	**24**	9.10E-05	1.18E-13
MI22	1657.17	3.52E+04	3.52E-14	1043.15	3.07E+09	**97**	7.50E-05	2.45E-14
MI24	1565.50	3.33E+04	3.33E-14	1043.15	2.90E+09	**92**	2.36E-04	8.17E-14
MI25	157.00	3.34E+03	3.34E-15	1043.15	2.90E+08	**9**	1.35E-04	4.65E-13
MI26	841.84	1.79E+04	1.79E-14	1043.15	1.56E+09	**49**	1.35E-04	8.67E-14

ORN-067_4

	ΔV	um^3	m^3	T (K)	Δt (s)	Δt (yr)		
MI1	468.17	9.95E+03	9.95E-15	1043.15	8.66E+08	**27**	1.38E-04	1.59E-13
MI3	377.67	8.03E+03	8.03E-15	1043.15	6.99E+08	**22**	1.34E-04	1.92E-13

ORN-067_5

	ΔV	um^3	m^3	T (K)	Δt (s)	Δt (yr)		
MI2	330.50	7.02E+03	7.02E-15	1043.15	6.11E+08	**19**	1.22E-04	2.00E-13
MI3	1938.67	4.12E+04	4.12E-14	1043.15	3.59E+09	**114**	2.43E-04	6.79E-14
MI4	280.67	5.97E+03	5.97E-15	1043.15	5.19E+08	**16**	1.07E-04	2.06E-13
MI6	145.17	3.09E+03	3.09E-15	1043.15	2.69E+08	**9**	2.30E-04	8.57E-13
MI7	1759.15	3.74E+04	3.74E-14	1043.15	3.25E+09	**103**	2.21E-04	6.78E-14

MI8	412.00	8.76E+03	8.76E-15	1043.15	7.62E+08	**24**	8.50E-05	1.12E-13
MI10	352.67	7.50E+03	7.50E-15	1043.15	6.52E+08	**21**	1.02E-04	1.56E-13

ORN-067_6

	ΔV	um^3	m^3	T (K)	Δt (s)	Δt (yr)		
MI1	351.16	7.46E+03	7.46E-15	1043.15	6.50E+08	**21**	1.06E-04	1.63E-13
MI2	150.17	3.19E+03	3.19E-15	1043.15	2.78E+08	**9**	8.68E-05	3.13E-13
MI3	183.33	3.90E+03	3.90E-15	1043.15	3.39E+08	**11**	8.93E-05	2.64E-13
MI4	203.33	4.32E+03	4.32E-15	1043.15	3.76E+08	**12**	8.91E-05	2.37E-13
MI5	187.50	3.99E+03	3.99E-15	1043.15	3.47E+08	**11**	1.01E-04	2.91E-13

ORN-067_11

	ΔV	um^3	m^3	T (K)	Δt (s)	Δt (yr)		
MI2	134.67	2.86E+03	2.86E-15	1043.15	2.49E+08	**8**	7.98E-05	3.21E-13
MI4	140.50	2.99E+03	2.99E-15	1043.15	2.60E+08	**8**	6.99E-05	2.69E-13

ORN-067_15

	ΔV	um^3	m^3	T (K)	Δt (s)	Δt (yr)		
MI3	223.17	4.74E+03	4.74E-15	1043.15	4.13E+08	**13**	1.06E-04	2.57E-13

F815-xl827

	ΔV	um^3	m^3	T (K)	Δt (s)	Δt (yr)		
MI5	574.50	1.22E+04	1.22E-14	1023.15	1.38E+09	**44**	1.58E-04	1.14E-13
MI6	39.00	8.29E+02	8.29E-16	1023.15	9.40E+07	**3**	2.60E-04	2.77E-12
MI7	515.50	1.10E+04	1.10E-14	1023.15	1.24E+09	**39**	2.28E-04	1.84E-13
MI8	319.67	6.79E+03	6.79E-15	1023.15	7.70E+08	**24**		
MI9	168.50	3.58E+03	3.58E-15	1023.15	4.06E+08	**13**		
MI12	1874.33	3.98E+04	3.98E-14	1023.15	4.52E+09	**143**	3.52E-04	7.79E-14
MI14	329.00	6.99E+03	6.99E-15	1023.15	7.93E+08	**25**	2.89E-04	3.65E-13
MI15	888.66	1.89E+04	1.89E-14	1023.15	2.14E+09	**68**	5.01E-04	2.34E-13
MI16	262.17	5.57E+03	5.57E-15	1023.15	6.32E+08	**20**	5.09E-04	8.07E-13
MI17	1181.34	2.51E+04	2.51E-14	1023.15	2.85E+09	**90**	4.47E-04	1.57E-13
MI18	2462.66	5.23E+04	5.23E-14	1023.15	5.93E+09	**188**	2.64E-04	4.94E-13
MI19	221.50	4.71E+03	4.71E-15	1023.15	5.34E+08	**17**		
MI21	130.50	2.77E+03	2.77E-15	1023.15	3.14E+08	**10**		
MI22	1057.50	2.25E+04	2.25E-14	1023.15	2.55E+09	**81**	3.39E-04	1.33E-13
MI24	106.17	2.26E+03	2.26E-15	1023.15	2.56E+08	**8**	3.40E-04	4.17E-13
MI25	338.84	7.20E+03	7.20E-15	1023.15	8.17E+08	**26**	2.98E-04	1.38E-13
MI26	895.33	1.90E+04	1.90E-14	1023.15	2.16E+09	**68**		

F815-xl830

	ΔV	um^3	m^3	T (K)	Δt (s)	Δt (yr)		
MI2	540.50	1.15E+04	1.15E-14	1023.15	1.30E+09	**41**	1.89E-04	1.45E-13
MI4	6495.28	1.38E+05	1.38E-13	1023.15	1.57E+10	**496**	2.06E-04	1.32E-14
MI11	222.17	4.72E+03	4.72E-15	1023.15	5.35E+08	**17**	2.11E-04	3.95E-13
MI12	435.00	9.25E+03	9.25E-15	1023.15	1.05E+09	**33**	2.20E-04	2.10E-13

F815-xl831

	ΔV	um^3	m^3	T (K)	Δt (s)	Δt (yr)		
MI3	205.17	4.36E+03	4.36E-15	1023.15	4.94E+08	**16**	2.03E-04	4.11E-13
MI7	517.00	1.10E+04	1.10E-14	1023.15	1.25E+09	**39**	1.73E-04	1.39E-13
MI8	1691.83	3.60E+04	3.60E-14	1023.15	4.08E+09	**129**	2.20E-04	5.41E-14
MI9	1925.83	4.09E+04	4.09E-14	1023.15	4.64E+09	**147**		
MI13	2738.03	5.82E+04	5.82E-14	1023.15	6.60E+09	**209**	1.69E-04	2.56E-14
MI14	277.83	5.91E+03	5.91E-15	1023.15	6.70E+08	**21**	1.53E-04	2.29E-13

MI15	216.00	4.59E+03	4.59E-15	1023.15	5.21E+08	**16**	1.20E-04	2.31E-13
MI18	1209.33	2.57E+04	2.57E-14	1023.15	2.91E+09	**92**	3.43E-04	1.18E-13
MI19	990.34	2.10E+04	2.10E-14	1023.15	2.39E+09	**76**	2.47E-04	1.04E-13
MI20	124.17	2.64E+03	2.64E-15	1023.15	2.99E+08	**9**	1.37E-04	4.59E-13
MI21	354.00	7.52E+03	7.52E-15	1023.15	8.53E+08	**27**	1.89E-04	2.22E-13
MI22	323.50	6.88E+03	6.88E-15	1023.15	7.80E+08	**25**	1.82E-04	2.33E-13
MI25	196.17	4.17E+03	4.17E-15	1023.15	4.73E+08	**15**	4.47E-04	9.46E-13
MI26	260.33	5.53E+03	5.53E-15	1023.15	6.27E+08	**20**		
MI28	130.33	2.77E+03	2.77E-15	1023.15	3.14E+08	**10**	5.02E-05	1.60E-13
MI29	212.83	4.52E+03	4.52E-15	1023.15	5.13E+08	**16**	2.52E-04	4.91E-13
MI32	1077.01	2.29E+04	2.29E-14	1023.15	2.60E+09	**82**	1.90E-04	7.33E-14

F815-xl013

	ΔV	**um^3**	**m^3**	**T (K)**	**Δt (s)**	**Δt (yr)**		
MI2	2209.83	4.70E+04	4.70E-14	1023.15	5.33E+09	**169**	2.91E-04	5.48E-14
MI8	106.67	2.27E+03	2.27E-15	1023.15	2.57E+08	**8**	1.73E-04	6.73E-13
MI10	234.00	4.97E+03	4.97E-15	1023.15	5.64E+08	**18**	4.60E-04	8.03E-13
MI12	238.00	5.06E+03	5.06E-15	1023.15	5.74E+08	**18**	4.60E-04	8.03E-13
MI13	1209.84	2.57E+04	2.57E-14	1023.15	2.92E+09	**92**	2.66E-04	9.12E-14
MI14	351.67	7.47E+03	7.47E-15	1023.15	8.47E+08	**27**	3.49E-04	4.13E-13
MI16	366.33	7.79E+03	7.79E-15	1023.15	8.83E+08	**28**	3.49E-04	3.96E-13
MI18	416.83	8.86E+03	8.86E-15	1023.15	1.00E+09	**32**	4.88E-04	4.86E-13
MI19	247.50	5.26E+03	5.26E-15	1023.15	5.96E+08	**19**	5.64E-04	9.47E-13
MI25	159.33	3.39E+03	3.39E-15	1023.15	3.84E+08	**12**	3.99E-04	1.04E-12
MI27	93.00	1.98E+03	1.98E-15	1023.15	2.24E+08	**7**	5.36E-04	2.39E-12
MI28	259.67	5.52E+03	5.52E-15	1023.15	6.26E+08	**20**	5.84E-04	9.34E-13
MI29	887.99	1.89E+04	1.89E-14	1023.15	2.14E+09	**68**	4.49E-04	2.10E-13
MI30	318.83	6.78E+03	6.78E-15	1023.15	7.68E+08	**24**	5.73E-04	7.47E-13
MI31	563.83	1.20E+04	1.20E-14	1023.15	1.36E+09	**43**	3.81E-04	2.81E-13
MI32	100.17	2.13E+03	2.13E-15	1023.15	2.41E+08	**8**	3.78E-04	1.57E-12
MI34	137.83	2.93E+03	2.93E-15	1023.15	3.32E+08	**11**	4.34E-04	1.31E-12
MI35	170.00	3.61E+03	3.61E-15	1023.15	4.10E+08	**13**	3.59E-04	8.76E-13
MI37	281.17	5.98E+03	5.98E-15	1023.15	6.78E+08	**21**	4.67E-04	6.90E-13
MI38	165.67	3.52E+03	3.52E-15	1023.15	3.99E+08	**13**	3.92E-04	9.82E-13
MI39	88.17	1.87E+03	1.87E-15	1023.15	2.12E+08	**7**	1.45E-04	6.84E-13
MI43	378.83	8.05E+03	8.05E-15	1023.15	9.13E+08	**29**	1.05E-04	1.16E-13
MI48	1108.83	2.36E+04	2.36E-14	1023.15	2.67E+09	**85**	1.01E-04	3.79E-14

BC17-Ia15_42

	ΔV	**um^3**	**m^3**	**T (K)**	**Δt (s)**	**Δt (yr)**		
MI2	298.00	6.33E+03	6.33E-15	1023.15	7.18E+08	**23**	1.38E-04	1.92E-13
MI3	272.67	5.80E+03	5.80E-15	1023.15	6.57E+08	**21**	9.01E-05	1.37E-13
MI4	487.00	1.04E+04	1.04E-14	1023.15	1.17E+09	**37**	8.98E-05	7.66E-14
MI5	199.67	4.24E+03	4.24E-15	1023.15	4.81E+08	**15**	1.30E-04	2.71E-13
MI12	366.50	7.79E+03	7.79E-15	1023.15	8.83E+08	**28**	9.67E-05	1.10E-13
MI13	178.17	3.79E+03	3.79E-15	1023.15	4.29E+08	**14**	1.09E-04	2.55E-13
MI17	540.50	1.15E+04	1.15E-14	1023.15	1.30E+09	**41**		
MI20	166.79	3.55E+03	3.55E-15	1023.15	4.02E+08	**13**	2.19E-04	5.46E-13
MI22	388.50	8.26E+03	8.26E-15	1023.15	9.36E+08	**30**	1.23E-04	1.32E-13
MI24	295.17	6.27E+03	6.27E-15	1023.15	7.11E+08	**23**	9.79E-05	1.38E-13

BC17-Ia15_43

	ΔV	**um^3**	**m^3**	**T (K)**	**Δt (s)**	**Δt (yr)**		
MI2	3111.83	6.61E+04	6.61E-14	1023.15	7.50E+09	**238**	2.50E-04	3.34E-14
MI3	2072.99	4.41E+04	4.41E-14	1023.15	5.00E+09	**158**	2.03E-04	4.06E-14

MI8	780.67	1.66E+04	1.66E-14	1023.15	1.88E+09	**60**	2.58E-04	1.37E-13
MI9	610.84	1.30E+04	1.30E-14	1023.15	1.47E+09	**47**	1.27E-04	8.64E-14
MI19	166.83	3.55E+03	3.55E-15	1023.15	4.02E+08	**13**		
MI21	396.34	8.42E+03	8.42E-15	1023.15	9.55E+08	**30**		

BC17-Ia15_44

	ΔV	**um^3**	**m^3**	**T (K)**	**Δt (s)**	**Δt (yr)**		
MI2	718.50	1.53E+04	1.53E-14	1023.15	1.73E+09	**55**		
MI3	220.50	4.69E+03	4.69E-15	1023.15	5.31E+08	**17**		
MI4	205.00	4.36E+03	4.36E-15	1023.15	4.94E+08	**16**	1.22E-04	2.47E-13
MI7	798.50	1.70E+04	1.70E-14	1023.15	1.92E+09	**61**	1.23E-04	6.42E-14
MI11	588.67	1.25E+04	1.25E-14	1023.15	1.42E+09	**45**	1.28E-04	9.01E-14
MI12	439.17	9.33E+03	9.33E-15	1023.15	1.06E+09	**34**		
MI13	485.00	1.03E+04	1.03E-14	1023.15	1.17E+09	**37**	2.84E-04	2.43E-13
MI14	310.33	6.60E+03	6.60E-15	1023.15	7.48E+08	**24**	2.53E-04	3.39E-13
MI15	417.33	8.87E+03	8.87E-15	1023.15	1.01E+09	**32**		
MI17	762.84	1.62E+04	1.62E-14	1023.15	1.84E+09	**58**	1.91E-04	1.04E-13
MI20	265.83	5.65E+03	5.65E-15	1023.15	6.41E+08	**20**	1.79E-04	2.80E-13
MI21	889.50	1.89E+04	1.89E-14	1023.15	2.14E+09	**68**	1.82E-04	8.51E-14

BC17-Ia15_45

	ΔV	**um^3**	**m^3**	**T (K)**	**Δt (s)**	**Δt (yr)**		
MI3	542.17	1.15E+04	1.15E-14	1023.15	1.31E+09	**41**	2.47E-04	1.89E-13
MI5	151.17	3.21E+03	3.21E-15	1023.15	3.64E+08	**12**		

BB08-21b_1

	ΔV	**um^3**	**m^3**	**T (K)**	**Δt (s)**	**Δt (yr)**		
MI9	155.33	3.30E+03	3.30E-15	1023.15	3.74E+08	**12**		
MI11	182.33	3.88E+03	3.88E-15	1023.15	4.39E+08	**14**	2.67E-04	6.08E-13
MI14	174.33	3.71E+03	3.71E-15	1023.15	4.20E+08	**13**		
MI29	611.50	1.30E+04	1.30E-14	1023.15	1.47E+09	**47**	1.62E-04	1.10E-13

BB08-21b_2

	ΔV	**um^3**	**m^3**	**T (K)**	**Δt (s)**	**Δt (yr)**		
MI1	124.17	2.64E+03	2.64E-15	1023.15	2.99E+08	**9**		
MI3	2214.83	4.71E+04	4.71E-14	1023.15	5.34E+09	**169**	2.39E-04	4.48E-14

BB08-21b_20a

	ΔV	**um^3**	**m^3**	**T (K)**	**Δt (s)**	**Δt (yr)**		
MI3	3562.48	7.57E+04	7.57E-14	1023.15	8.58E+09	**272**	2.74E-04	3.20E-14

BB08-21b_20b

	ΔV	**um^3**	**m^3**	**T (K)**	**Δt (s)**	**Δt (yr)**		
MI7	510.17	1.08E+04	1.08E-14	1023.15	1.23E+09	**39**	2.32E-04	1.88E-13
MI9	257.67	5.48E+03	5.48E-15	1023.15	6.21E+08	**20**	2.52E-04	4.05E-13
MI10	1140.66	2.42E+04	2.42E-14	1023.15	2.75E+09	**87**	1.32E-04	4.82E-14

BB08-21b_22

	ΔV	**um^3**	**m^3**	**T (K)**	**Δt (s)**	**Δt (yr)**		
MI1	334.50	7.11E+03	7.11E-15	1023.15	8.06E+08	**26**		
MI3	454.67	9.66E+03	9.66E-15	1023.15	1.10E+09	**35**		
MI6	230.17	4.89E+03	4.89E-15	1023.15	5.55E+08	**18**		
MI8	244.00	5.19E+03	5.19E-15	1023.15	5.88E+08	**19**	2.09E-04	3.56E-13
MI9	135.50	2.88E+03	2.88E-15	1023.15	3.27E+08	**10**		
MI10	500.83	1.06E+04	1.06E-14	1023.15	1.21E+09	**38**	1.64E-04	1.36E-13